JGR Atmospheres

RESEARCH ARTICLE
10.1029/2022JD037454

Key Points:

- Ensemble data assimilation of Geostationary Operational Environmental Satellite Series-R aerosol optical depth (AOD) retrievals for short-term smoke forecasts
- Assimilation of AOD improves the forecast of smoke aerosols in two wildfire cases
- Improved smoke forecasts impact forecasts of the surrounding atmospheric conditions

Correspondence to:
T. Jones,
Thomas.Jones@noaa.gov

Citation:
Jones, T., Ahmadov, R., & James, E. (2022). Assimilation of aerosol optical depth into the Warn-on-Forecast System for Smoke (WoFS-Smoke). *Journal of Geophysical Research: Atmospheres*, *127*, e2022JD037454. https://doi.org/10.1029/2022JD037454

Received 6 JUL 2022
Accepted 6 DEC 2022

Author Contributions:
Conceptualization: Thomas Jones
Data curation: Thomas Jones
Formal analysis: Thomas Jones
Funding acquisition: Thomas Jones
Investigation: Thomas Jones
Methodology: Thomas Jones, Ravan Ahmadov, Eric James
Project Administration: Thomas Jones
Resources: Thomas Jones
Software: Thomas Jones, Ravan Ahmadov, Eric James
Supervision: Thomas Jones
Validation: Thomas Jones
Visualization: Thomas Jones
Writing – original draft: Thomas Jones
Writing – review & editing: Thomas Jones

Assimilation of Aerosol Optical Depth Into the Warn-on-Forecast System for Smoke (WoFS-Smoke)

Thomas Jones[1,2,3], Ravan Ahmadov[4,5], and Eric James[4,5]

[1]Cooperative Institute for Severe and High-Impact Weather Research and Operations, University of Oklahoma, Norman, OK, USA, [2]NOAA/National Severe Storms Laboratory, Norman, OK, USA, [3]School of Meteorology, University of Oklahoma, Norman, OK, USA, [4]Cooperative Institute for Research in Environmental Sciences, University of Colorado, Boulder, CO, USA, [5]NOAA/OAR/Global Systems Laboratory, Boulder, CO, USA

Abstract This research extends the Warn-on-Forecast System for Smoke (WoFS-Smoke) by adding the capability to assimilate aerosol optical depth (AOD) retrievals from the Geostationary Operational Environmental Satellite Series-R (GOES-R) satellites. The WoFS is a rapidly cycling, ensemble-based analysis and forecasting system designed to generate short term (0–3 hr) forecasts of high impact weather. WoFS-Smoke provides short-term forecasts of smoke aerosols injected into the atmosphere from ongoing wildfires. The vertically integrated concentration of smoke aerosols in the atmosphere can be estimated from satellite based AOD retrievals. To assimilate AOD into WoFS-Smoke, a smoke control variable is added to the prognostic state that is updated during each assimilation cycle. Then, a forward operator is created to relate modeled smoke aerosols to AOD retrievals using a mathematical function developed for the smoke-AOD conversion used by the High-Resolution Rapid Refresh for Smoke. Finally, GOES-R AOD retrievals are quality controlled and are assimilated at 15 min intervals. Comparing analyzed AOD with smoke and other atmospheric variables indicates that assimilating AOD not only directly impacts smoke aerosol concentration in the system, but also has indirect impacts on variables such as temperature, humidity, and wind. Results from two wildfire cases in Oklahoma and Arizona show that assimilating AOD substantially impacts the concentration and distribution of smoke aerosols in the system. Forecast verification against satellite and surface observations indicates the overall impact of assimilating AOD in WoFS-Smoke can improve forecast skill of smoke and the surrounding environment.

Plain Language Summary Short-term forecasts of smoke generated from the Warn-on-Forecast System for Smoke (WoFS-Smoke) data assimilation and forecasting system are improved through the assimilation of aerosol characteristics derived from satellites. Satellite measurements of aerosols provide information on the amount and distribution of aerosols in the atmosphere. Assimilating these data into a system designed to track smoke aerosols produces a more accurate analysis of smoke concentration. This work uses aerosol observations from a geostationary orbiting satellite to take advantage of the high temporal frequency (<15 min) needed to continuously update smoke in WoFS-Smoke. Testing of two wildfire events showed that assimilating aerosol characteristics improved both smoke forecasts and forecasts of the surrounding atmospheric conditions.

1. Introduction

Aerosols of various types (dust, sulfates, black carbon, etc.) affect surrounding atmospheric conditions by blocking solar radiation reaching the surface (Benedetti et al., 2019; Iacono et al., 2004; Kochanski et al., 2019; Lareau & Clements, 2015; Mlawer et al., 1997; Robock, 1988, 1991; Textor et al., 2006, 2007), acting as cloud condensation nuclei (e.g., Fromm et al., 2006, 2010, 2016; Mann et al., 2014; Twomey, 1977), and reducing overall air quality (e.g., Pandolfi et al., 2014; Pope et al., 2002). Assimilation of aerosol properties into numerical weather prediction (NWP) models is important so that these effects to the atmospheric state can be accurately forecast. Most operational global models assimilate aerosol information retrieved from satellite data and climatological analyses (e.g., Benedetti et al., 2009). Several methods for assimilating aerosol properties exist and include variational (Chen et al., 2017; Liu et al., 2011; Saide et al., 2013, 2014) and ensemble techniques using either satellite and/or surface-based observations (e.g., Peng et al., 2017; Rubin et al., 2016, 2017; Sekiyama et al., 2010; Tsikerdekis et al., 2020; Yumimoto et al., 2016). Choi et al. (2020) evaluated 3D-VAR, ensemble, and hybrid methods for assimilating dust aerosol optical depth (AOD) over the eastern Atlantic and western Africa. Their

conclusions indicated that ensemble and hybrid assimilation techniques showed clear advantages over traditional variational methods when verified against aerosol observations. Sekiyama et al. (2010) used an ensemble Kalman filter (EnKF) approach to assimilate aerosol characteristics retrieved from the CALIPSO satellite to improve forecasts of dust aerosols over Japan. Most of these studies utilize data from polar orbiting satellites, which are adequate for global forecasting needs, but do not have the temporal resolution necessary for regional, convection allowing models (CAMs). Saide et al. (2014) and Yumimoto et al. (2016) tested the assimilation of aerosol properties derived from the Himawari-8 geostationary satellite and found some improvement in the aerosol and air quality forecasts compared to only assimilating data from polar orbiting satellites in Japan. As expected, the higher temporal resolution and spatial coverage afforded by geostationary based sensors can provide significant advantages to NWP systems.

Assimilation of aerosol properties into CAMSs has not been prioritized until recently. Back et al. (2020) tested the assimilation of Visible Infrared Imaging Radiometer Suite (VIIRS) AOD retrievals to improve forecasts of smoke generated by wildfires into the High-Resolution Rapid Refresh for Smoke (HRRR-Smoke). HRRR-Smoke is a CAM with a 3 km grid spacing and is cycled hourly over a Continental United States (CONUS) domain (Ahmadov et al., 2017; Dowell et al., 2022; James et al., 2022). However, AOD assimilation into a limited area domain, rapidly cycled (sub hourly) forecast system designed for an operational framework has yet to be fully explored. One such system is the Warn-on-Forecast System (WoFS) initially designed to generate short-term (0–6 hr) forecasts of high impact weather events such as storm rotation, large hail, severe winds, and flash flooding (Jones et al., 2016; Skinner et al., 2018; Stensrud et al., 2009, 2013; Wheatley et al., 2015; Yussouf & Knopfmeier, 2019). Recently, Jones et al. (2022) extended the WoFS to ingest fire radiative power (FRP) retrievals of wildfires to initiate smoke plumes within the system using the smoke plume injection algorithm created for HRRR-Smoke. Results from this work showed that WoFS-Smoke generated reasonably accurate probabilistic forecasts of smoke plumes associated with several large wildfires occurring in the western CONUS during the summer of 2020 when compared against surface, satellite, and radar observations. However, certain limitations were also noted which included errors in the concentration and spatial extent of the smoke plumes in the forecasts.

In an effort to address these limitations, we develop an AOD assimilation capability for WoFS-Smoke. WoFS uses an EnKF assimilation technique and cycles at 15 min intervals, so this system combines the favorable attributes of ensemble data assimilation with high frequency remote sensing data. AOD and aerosol type (dust or smoke) products are retrieved in realtime using infrared and visible channel data from GOES-R. This work focuses on extending WoFS-Smoke with the necessary forward operator and state variables needed to fully assimilate AOD along with the radar (reflectivity and radial velocity) and satellite (water vapor radiances and cloud water path (CWP)) data used in the existing system. To assess the impact of assimilating AOD from smoke, sensitivity analysis are performed for two wildfire cases (one in Oklahoma and one in Arizona) comparing no-AOD to AOD assimilation experiments. Cases were selected based on a desire for testing isolated smoke plumes, the availability of initial conditions, quality of AOD retrievals, and for one case the presence of high density surface observations. Qualitative and quantitative verification is performed using observed AOD, visible imagery, and surface measurements of incoming solar radiation. The goal is to provide evidence that assimilating AOD into WoFS-Smoke increases skill in smoke forecasts as well as its thermodynamic impact on the surrounding environment.

Following the Section 1, the WoFS-Smoke configuration, the AOD retrievals and development of the forward operator are discussed in Section 2. Section 3 provides case summaries for each fire. Section 4 describes the covariance characteristics between analyzed AOD and other model variables as well as bias and error characteristics for assimilated AOD. Section 5 discusses qualitative and quantitative comparisons of each AOD assimilation experiment, with conclusions following in Section 6.

2. WoFS-Smoke Description

2.1. System Configuration

The baseline configuration of the WoFS is described in detail by Wheatley et al. (2015), Jones et al. (2016, 2020), and Skinner et al. (2018). A regional domain is selected daily and encompasses the area of expected high impact weather. The WoFS is initialized in the mid-morning from the HRRR 36 member ensemble and cycled at 15 min intervals thereafter assimilating all available conventional (temperature, humidity, wind, pressure), radar (WSR-88D reflectivity and Doppler radial velocity), and geostationary satellite observations (CWP, clear

sky radiances). Boundary conditions are provided by a 9 member HRRR-ensemble forecast initiated daily at 1200 UTC. WoFS forecasts are generated from the updated analyses at hourly or sub-hourly intervals. In the WoFS-Smoke configuration used here, smoke aerosol concentrations are initialized from the HRRR-Smoke analysis corresponding to the system initialization time and smoke boundary conditions are set to zero (Jones et al., 2022). As of 2022, WoFS-Smoke has a horizontal grid spacing of 3 km with a domain 900 × 900 km in size and 51 vertical levels extending from the surface up to a model top of ∼20 hPa.

Data are assimilated for the duration of each case using the EnKF technique and utilizing the forward operators included within the Community Gridpoint Statistical Interpolation (GSI) software (Hu et al., 2016; Kleist et al., 2009; Whitaker et al., 2008). The WoFS uses the Advanced Weather Research and Forecasting model (WRF-ARW) version 3.9.1, similar to the version used by the HRRRv4 (Powers et al., 2017; Skamarock et al., 2008). Jones et al. (2022) extended WoFS into the WoFS-Smoke configuration by adding the smoke plume injection algorithm from HRRR-Smoke into the system (Freitas et al., 2006, 2007). The Freitas et al. (2006, 2007) estimates plume rise using a 1-D entrainment parameterization scheme that incorporates model data (temperature, moisture, horizontal and vertical velocity, cloud hydrometeor variables, and land surface conditions) at each model grid point. Vertical velocity within this column is estimated using these data combined with the FRP observation at that location. Smoke injection height is then calculated and transferred back to the NWP model (e.g., WRF), which uses this information to release aerosols into the model analysis. For wildfires encompassing multiple grid points that have large variations in size and intensity, multiple injection heights may be associated with an individual fire resulting in a complex vertical distribution of aerosols at the analysis time.

To enable assimilation of AOD retrievals, the smoke aerosol tracer is added to the set of prognostic state variables updated during each assimilation cycle (Choi et al., 2020). The EnKF updates a predefined set of prognostic variables during the assimilation process nominally consisting of parameters such as temperature, humidity, pressure, wind, and hydrometeors. The addition of a smoke variable allows smoke concentrations to be directly updated through assimilation of AOD retrievals. When AOD is not being assimilated, the smoke state variable is retained to maintain a consistent WoFS-Smoke configuration. Without AOD assimilation, adding smoke to the updated state has little impact since no other assimilated observations are highly correlated with smoke concentrations. Smoke plumes from wildfires are initiated and updated using the Freitas method described above. WoFS-Smoke currently ingests FRP retrievals from the Suomi-NPP, NOAA-20, Terra, and Aqua satellites at hourly intervals (Ahmadov et al., 2017; Jones et al., 2022). A full description of this processes is provided in Jones et al. (2022).

2.2. AOD Assimilation

Aerosols lofted into the atmosphere are detectable from satellite sensors such as the Moderate Resolution Imaging Spectroradiometer, VIIRS, and Advanced Baseline Imager (ABI), using visible and infrared bands (e.g., Coakley et al., 1983; Kaufman et al., 1997; Remer et al., 2005). AOD represents the extinction of solar radiation as it passes through the atmosphere due to aerosol particles such as sulfates, dust, black carbon, and sea-salt. Retrieval algorithms function by matching the observed reflectance values to expected values based on lookup tables generated from radiative transfer models (RTMs) for various aerosol types. Then, AOD is retrieved where the best fit match is made. An AOD near to zero indicates a pristine, aerosol-free environment with values greater than 1.0 indicating very heavy aerosol concentrations. Since AOD is a total-column product, no information on the vertical distribution of aerosols is present. Retrievals are made primarily using visible channels, so aerosol data are generally not available during nighttime hours using these methods. Larger uncertainties in AOD occur over bright surfaces such as deserts (e.g., Levy et al., 2007) or in the vicinity of clouds (e.g., Koren et al., 2007; Zhang et al., 2005). The latter limitation is critical since smoke from intense wildfires is often co-located with pyro-cumulus (pyroCu). This work uses the level 2 (L2) AOD product, CONUS domain (AODC) generated in realtime from GOES-R data. The GOES-R AOD retrieval algorithm was developed to use the visible and infrared reflectances observed by the ABI to retrieve AOD at 0.55 μm and aerosol type for full-disk and CONUS domains. Retrievals are made at an effective resolution of 2 km at 5 min intervals in the CONUS domain product. Cloudy pixels are filtered out prior to applying the AOD retrieval algorithm to remove potential cloud contamination in the product. Valid AOD retrievals for both cases range from 0 to 2.5.

To assimilate AOD into the system, it is important to develop a robust forward operator that simulates model AOD values from an analyzed atmospheric state. Many recent AOD assimilation efforts have utilized a RTM to relate the analyzed atmospheric state (including aerosol concentrations and clouds) to retrieved properties such

as AOD (e.g., Choi et al., 2020; Liu et al., 2011). While this method has proven successful for many applications, the assumptions used for aerosol type and surrounding cloud properties may not be completely suitable as a forward operator for our application. Initial testing of this method generated undesirable biases and errors, which significantly limited the potential for successfully assimilating AOD in WoFS-Smoke. For example, a very high positive bias in synthetic AOD was generated using this method while also having a substantial variability from cycle to cycle. Potential reasons include the model aerosol type not fully matching the assumptions present in the RTM and small variations in smoke concentrations having an outsized impact using this method. Attempting to address these and other uncertainties lies outside the scope of this work and left for future research.

Instead of using the Community Radiative Transfer Model included in the GSI software as the forward operator, this work uses a mathematical relationship between 3-D smoke aerosol concentrations and AOD at 0.55 μm established by Randles et al. (2017). First, an extinction coefficient (ext) is defined by summing two constants sc_me = 4 and ab_me = 0.5 corresponding to the scattering and absorption efficiency for smoke respectively. At each grid point and model level, a moisture adjustment is then applied to this coefficient (aext) when relative humidity (RH) > 30% to account for hydroscopic aerosol growth (Equation 1). Synthetic AOD between 2 model levels (AOD[z]) is then calculated by multiplying the smoke aerosol mixing ratio ($PM_{2.5}$), RH, the height between model levels (dZ), and the adjusted extinction coefficient (aext) as shown in Equation 2.

$$\text{aext} = \text{ext} \times \left(\frac{1 - 0.3}{1 - \text{RH}[z]} \right)^{0.18} \tag{1}$$

$$\text{AOD}[z] = 10^{-6} \times \text{aext} \times \text{PM}_{2.5}[z] \times \text{RH}[z] \times (dZ) \tag{2}$$

Finally, total column AOD for a model grid point is calculated by integrating AOD[z] over all model levels (Equation 3).

$$\text{AOD} = \sum_{z=0}^{\text{model-top}} \text{AOD}[z] \tag{3}$$

Randles et al. (2017) applied this formula for in successful AOD assimilation experiments using the Goddard Aerosol Assimilation System.

Synthetic AOD values greater than 2.5 are set to 2.5 to correspond with the maximum possible retrieval value, accounting for ~10% of the data. A similar adjustment is applied to CWP in the baseline WoFS system since the retrievals CWP retrievals saturate in thick clouds and precipitation (Jones et al., 2016). Tracers for other aerosol types are not included in this version of WoFS-Smoke and do not contribute to the synthetic AOD values produced.

GOES-R AOD retrievals must also be processed from their raw state prior to assimilation. As with other satellite observations such as CWP and radiances (Jones et al., 2016, 2020), AOD data are thinned to a 5 km resolution. Non-smoke AOD retrievals classified by the L2 Aerosol Detection Product, CONUS domain (ADPC) are also filtered out at this time. Since AOD is a very non-linear variable, applying a single observation error for all observations would not be optimal (Choi et al., 2020; Schwartz et al., 2014). Thus, we apply the same approach used for CWP and vary the observation error as a function of the retrieved AOD value from 0.025 up to 0.85. Using this approach allows for low AOD values to have a meaningful impact during the assimilation process while not overfitting the model where high AOD values are present. As with other satellite and radar variables, horizontal and vertical localization values that use the Gaspari and Cohn (1999) technique are also applied. Testing showed that a horizontal localization radius of 36 km, the same as currently used for CWP and radiance observations, performed well. Overall sensitivity of the horizontal localization radius to the impact of AOD assimilation was low between the ranges of 20–50 km. Assigning a vertical localization is more complicated. Since AOD is a vertically integrated value, applying a specific vertical level and localization radius is not practical. We chose to assume an infinite vertical localization similar to that used for radiance observations in the system. Since AOD observations, much like radiances, have no assigned vertical level, we must allow the opportunity for AOD observations to impact all model levels, not just a few levels near the surface or high in the atmosphere. When considering the complex vertical profile of smoke aerosol concentrations, it is vital that the assimilation methods used here can adjust these profiles in a realistic manner.

Another concern are biases in the AOD observations and synthetic AOD calculation. As with other observation types, large biases in one or the other can lead to non-optimal assimilation of these data. Applying a bias correction is not trivial and requires extensive knowledge of the bias characteristics of AOD from thick smoke. AOD retrievals and synthetic model analysis were compared to determine if a consistent bias was detectable. Results indicated large differences in bias characteristics from various cases for AOD > 0.25 (not shown); thus, we decided not to apply a bias correction for the following experiments. A larger sample of cases will be used in the future to further assess potential bias corrections in follow-up work.

For the 2018 case, the system is initialized at 1800 UTC and cycled at 15 min intervals until 0100 UTC. The 2020 case is similar, but initialized at 1500 UTC while also ending at 0100 UTC. All experiments assimilate conventional, radar reflectivity and radial velocity observations as in Jones et al. (2022). For this work, no radiance or CWP data are assimilated. The current clear-sky radiance and CWP observations used in WoFS do not include areas of significant aerosol coverage. In both cases, they are masked out during the observation pre-processing phase. Assimilating either would provide no additional aerosol information to the system. Ensemble forecasts are generated at selected analysis times starting at 2000 UTC. Two sets of experiments are conducted. The control experiment (CNTL) contains smoke initiated from FRP retrievals, but does not assimilate AOD. The second experiment with AOD (WAOD) follows the CNTL configuration, but also assimilates GOES-16 AOD retrievals at 15 min intervals. The primary goal of comparing these experiments is to determine under what circumstances assimilating AOD can improve both smoke forecasts and forecasts of the surrounding environment.

3. Wildfire Case Overviews

3.1. 13 April 2018

On 13 April 2018, a sharp dryline moved eastward through Oklahoma with severe thunderstorms generated ahead and very dry, windy conditions being present behind. The strong westerly winds coupled with the extremely dry airmass resulted in an environment favorable for wildfires. Several large grassfires initiated in northwestern OK during the early afternoon and continued into the evening (Figure 1a). FRP retrievals from GOES-16 and polar orbiting satellites within this domain show the spatial extent of these fires. The largest complex occurs in the central portion of the domain with a secondary fire further to the southwest. GOES-16 FRP retrievals also reveal many small, short-lived fires. Total GOES-16 FRP begins to increase at 1730 UTC peaking at around 2000 UTC before rapidly decreasing to near zero by 0000 UTC. Retrievals from polar-orbiting sensors only provide data between 1730 and 2000 UTC; thus, they do not sample the temporal evolution of these fires. At 2100 UTC, visible (0.47 μm) GOES-16 imagery shows smoke plumes emanating from the ongoing wildfires being advected in a northeasterly direction by the environmental flow (Figure 2a). Smoke from both large fires combined to form one large smoke plume by 2100 UTC. The coverage of smoke increases over the next 90 min (Figures 2b and 2c). Corresponding AOD retrievals also show the extent of the smoke with large areas of AOD > 0.5 during this period (Figures 2d–2f). However, note that AOD retrievals were not made in the areas of greatest aerosol concentrations owing to being miss-classified as clouds.

3.2. 16 June 2020

On 16 June 2020, a large wildfire was ongoing in central AZ that is known as the Bush fire. Dry conditions had been present in much of the AZ during the previous weeks, resulting in large areas of dry brush suitable to sustain large fires. Satellite FRP retrievals show the crescent shaped fire line with the GOES-16 FRP time-series indicating the maximum intensity of the fire is occurring between 2000 and 0000 UTC (Figure 1b). By 2200 UTC a large smoke plume extends northeastward from the fire which eventually reaches in to western New Mexico by 0100 UTC 17 June 2020 (Figures 3a–3c). A second fire, known as the Mangum fire, was also ongoing in the northwestern portion of the domain generating large amounts of smoke in southern Colorado. AOD retrievals are made for large portions of both smoke plumes, though few AOD retrievals are associated with the Mangum fire until after 2300 UTC (Figures 3d–3f). One consistent issue with the AOD retrievals in both AZ fires are missing retrievals in the thickest portions of the smoke plume. We chose to use GOES-16 rather than GOES-17 AOD retrievals for this work since the latter had difficulty in generating valid retrievals in northeastern AZ.

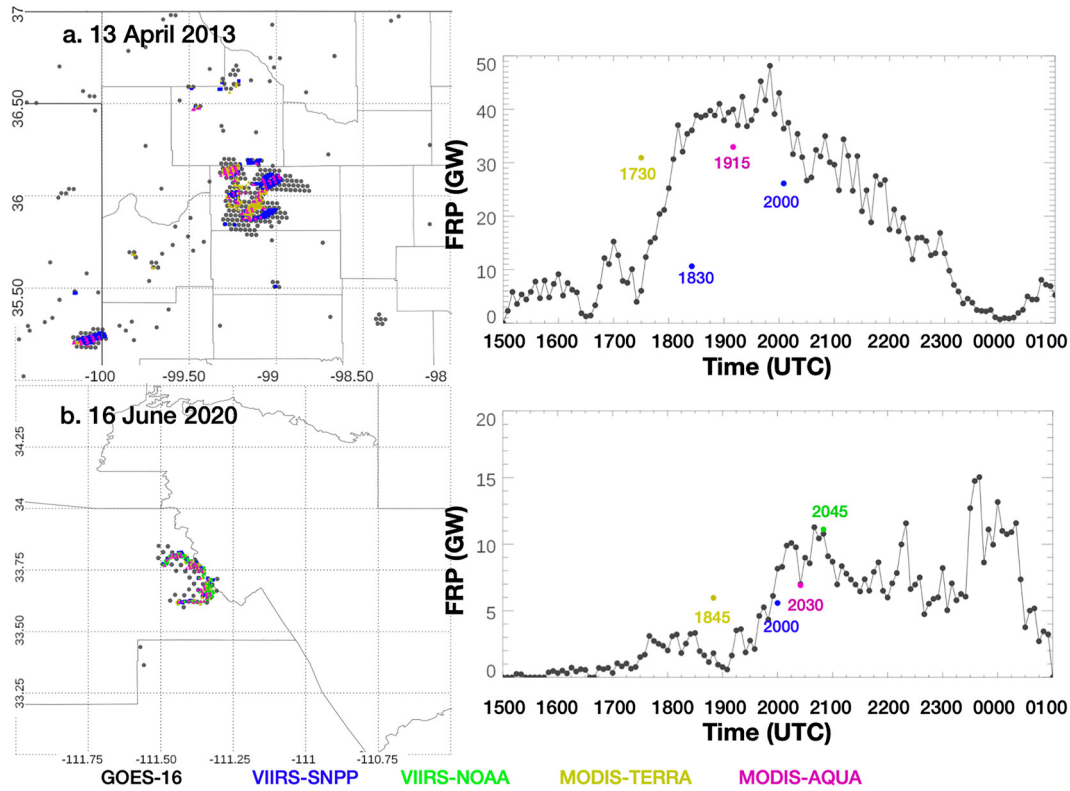

Figure 1. The left column shows hotspot retrievals between 1500–0100 UTC from the Terra, Aqua, Suomi-NPP, NOAA-20 and GOES-16 satellites for the 13 April 2018 (a) and 16 June 2020 (b) cases. GOES-16 retrievals are plotted at their native resolution of 2 km, with data from the other sensors having a finer resolution. The right column shows the sum of fire radiative power for all retrievals within a 5 min window from each satellite in this domain over the same time period.

4. Observation Diagnostics

4.1. Covariance Analysis

Before analyzing the case-study results, it is important to analyze the expected impact of assimilating AOD on the model state. To assess how assimilating AOD relates to individual atmospheric variables, the covariance between synthetic AOD and selected variables including PM2.5 (smoke), temperature (T), humidity (Qv), and meridional wind (V) are calculated. The covariance at each model grid point is calculated by comparing the AOD analysis from each ensemble member to the value of the atmospheric variable at that grid-point for each member, resulting in a 2×36 array at each point. Since AOD is a 2-D parameter, the same value is used in computing the covariance between it and the atmospheric variable for all model levels at a given location. Cross-sections of the resulting 3-D covariances fields are created along the forecast smoke plumes for both cases. These plots indicate how 2-D AOD retrievals will contribute to changes in the 3-D distribution of smoke in the model, which are the greatest where the covariances values are highest.

On 13 April 2018 at 2100 UTC, model derived AOD is strongly correlated with 3-D smoke along the line of maximum smoke concentration. Figure 4a shows the AOD-smoke covariance at ~2 km above the surface. A vertical cross section of the covariance field across this line shows positive covariance values between AOD both near the surface and over 4 km above the surface (Figure 4b). Given that AOD is calculated directly from smoke, such high covariances values would be expected. More interesting are indirect relationships between AOD and non-smoke variables. For temperature, the overall covariance values are much lower, but some relationship between these fields is evident (Figure 4c). Note that the sign of perturbation potential temperature was reversed for these plots so that positive covariances values would correspond to atmospheric cooling. Larger AOD values are associated with cooling at multiple atmospheric levels, which would be expected (Figure 4d). A somewhat unexpected result was a positive relationship found between AOD and atmospheric water vapor (Figures 4e and 4f). For this case, AOD and water vapor are positively correlated in the area of the largest fire, with positive

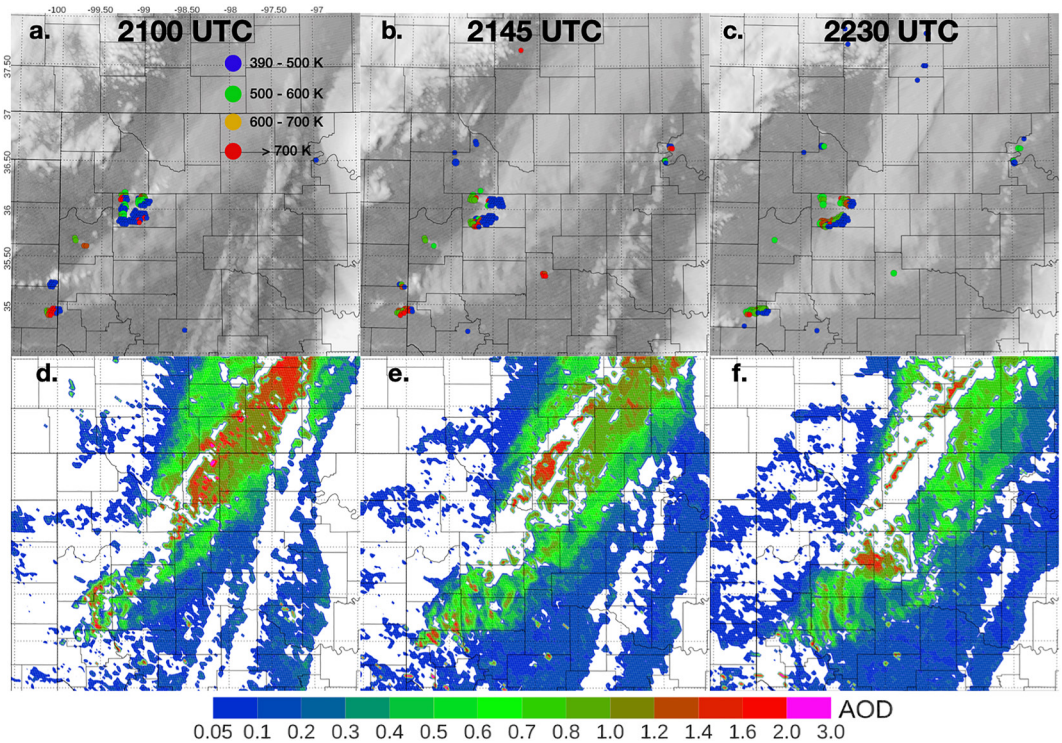

Figure 2. GOES-16 visible (0.47 μm) imagery at 2100, 2145, and 2230 UTC on 13 April 2018 (a–c). Corresponding fire radiative power retrievals from GOES-16 at these times are also provided with colors representing their retrieved temperature and their size as a representation of their coverage. The size of the dots does not directly represent the actual fire size, but is plotted to show the locations of smaller versus larger detections. The bottom row of plots shows GOES-16 aerosol optical depth retrievals at these times (d–f). Note that few retrievals exist near the areas of highest smoke concentrations due to these areas being classified as "clouds".

correlation extending to 4 km above the surface (Figure 4f). Thus, assimilating AOD even where little smoke exists in the model analysis may act to increase atmospheric moisture. Finally, the covariance between meridional wind and AOD was examined. Positive values are generally present on the northwest side of the analyzed smoke plume and low to negative values to the southeast (Figure 4g). The vertical cross section shows the impact varies significantly with height with both a low-level and upper-level maxima (Figure 4h). The exact mechanism for the upper-level (10–12 km) positive covariance values remains unclear. Covariances characteristics associated with zonal wind are similar (not shown). The covariance patterns associated with the 16 June case are consistent with the 13 April case, but with the covariance between AOD and the other atmospheric variables is generally larger (Figure 5). This is due to the much higher analyzed smoke concentrations compared to the 13 April case and the smoke emanating from a single, large fire in the plotted domain. Covariance calculations were done for several other cases, and all generated similar patterns (not shown). Having the covariance characteristics of these cases being very similar provides confidence that the impact of assimilating AOD will be consistent from case to case. These statistical analyses are vital to understanding how assimilating AOD impacts the overall forecast system and under what conditions assimilating AOD data is likely to have its greatest effect.

4.2. Assimilated AOD Retrievals

The number of AOD observations assimilated is driven by several factors including the coverage of existing smoke plumes, the surrounding environmental aerosol loading, and the quality of the AOD retrievals in changing conditions. For the 13 April 2018 case, the cycling starts at 1800 UTC at which time the smoke plumes are relatively small resulting in few AOD retrievals (Figure 6a). This number increase rapidly, peaking above 2500 between 2200 and 2300 UTC corresponding to the rapid expansion of the smoke plumes. After 2300 UTC, the number of retrievals begin to decrease as darkness begins to fall across the domain and the fires weaken. On 16 June 2020, the number of AOD retrievals assimilated at the first cycle of 1500 UTC is in excess of 4000 and

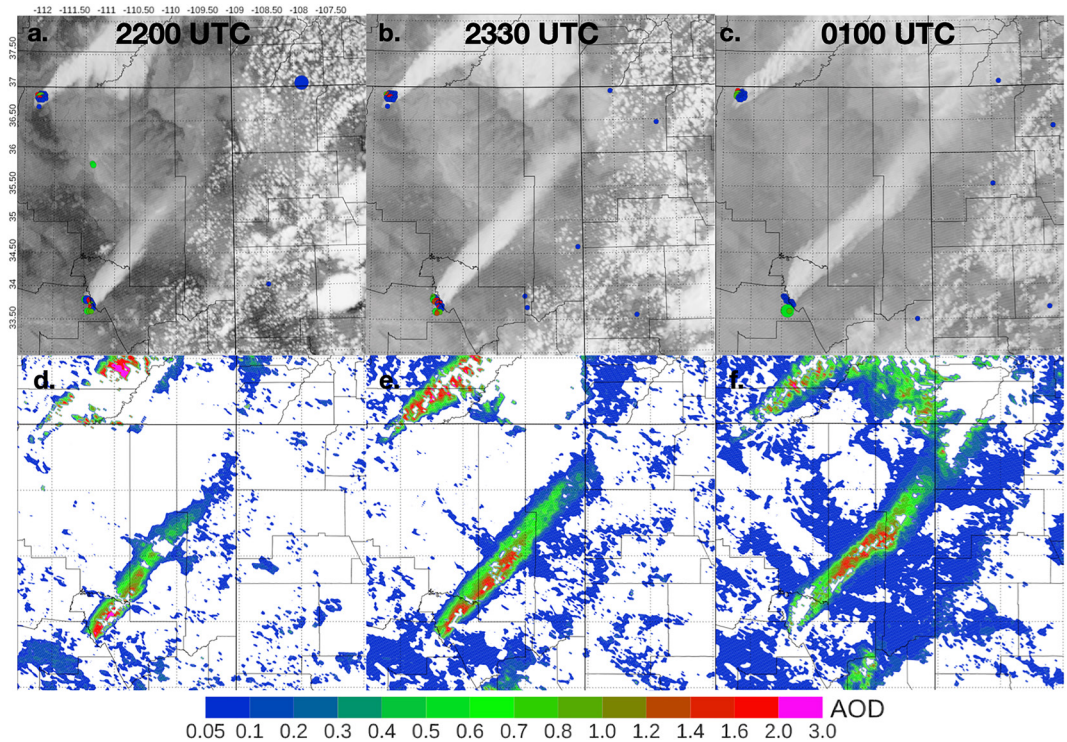

Figure 3. Same as Figure 2, but for 16–17 June 2020 at 2200, 2330, and 0100 UTC.

gradually decrease until 2000 UTC (Figure 6c). These AOD retrievals generally represent existing aerosols in the atmosphere not associated with the ongoing fires. After 2000 UTC, the smoke coverage grows increasing the number of AOD retrievals assimilated during the remainder of the cycling period.

The bias, root mean square error (RMSE), and total spread (SPRD) are calculated at each cycle to assess the adjustment resulting from AOD assimilation. On 13 April, both bias and SPRD are quite large (>0.4) between 1800–2100 UTC (Figure 6b). Bias is defined as the observation minus the analysis (o-a) with positive values indicating the model is underestimating AOD. Despite FRP retrievals being ingested at 1730 and 1830 UTC, time is still required to transport smoke from these fires downstream from the source into the surrounding environment. Bias and RMSE decrease until 2300 UTC as the impact of assimilating the AOD retrievals builds up over time. RMSE and SPRD also begin to converge indicating that the retrievals are being assimilated more optimally during this period. On 16 June 2020, extensive aerosol coverage exists both in the observations and model initial conditions at 1500 UTC with the model having a low bias in aerosol concentration (Figure 6d). However, the overall aerosol concentrations are low, resulting in relatively small impacts from assimilation until 2000 UTC. These impacts increase afterward as AOD retrievals associated with the smoke plumes become more evident leading to a larger number of high AOD values (>0.5) being assimilated. By 2300 UTC, the RMSE and SPRD values are similar indicating that the assimilation has a reached a more optimal state.

Maintaining ensemble spread when assimilating AOD is a challenge also noted by Rubin et al. (2016), Schwartz et al. (2014) and Choi et al. (2020). The initial WoFS-Smoke system described by Jones et al. (2022) did a reasonable job with spread in the intensity of smoke aerosols, but not their location. The main challenge is that fires are considered stationary sources of smoke with little short-term trend information being included. If smoke is injected into an atmospheric layer where little member to member variation exists, there is limited opportunity for the extent of the smoke transport to differ between these members. Ongoing work aims to further improve the potential for aerosol spread in the system, which should allow for more optimal AOD assimilation in future versions of WoFS-Smoke. Still, this work represents an important first step in assimilating AOD into ensemble based high resolution forecast system. Further optimization of the system is expected as ongoing research explores more cases and adjustments to the AOD data assimilation techniques.

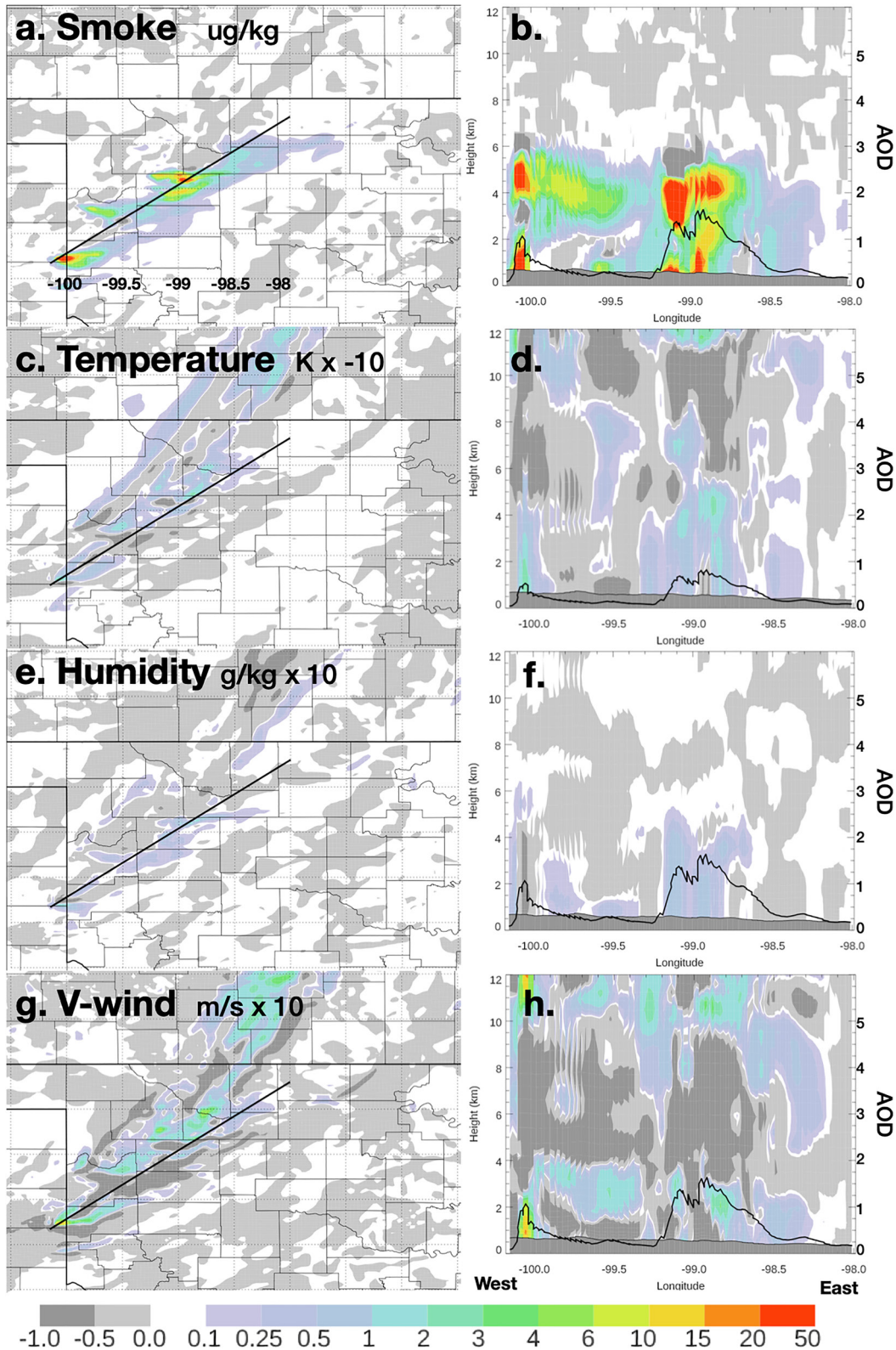

Figure 4. Ensemble covariance plots between analyzed 2-D aerosol optical depth (AOD) and smoke (a), perturbation potential temperature (c), water vapor mixing ratio (e), and the meridional component of wind (g) at 800 hPa at 2100 UTC 13 April. The cross-section of ensemble covariance is provided for each variable (b, d, f, h) along a southwest to northeast path correspond to the location of the main smoke plumes. Covariance values are multiplied by a factor of −10, 10, and 10 for temperature, humidity, and zonal wind to accentuate the differences. The black line on the cross-section plots represents the ensemble mean AOD along this path.

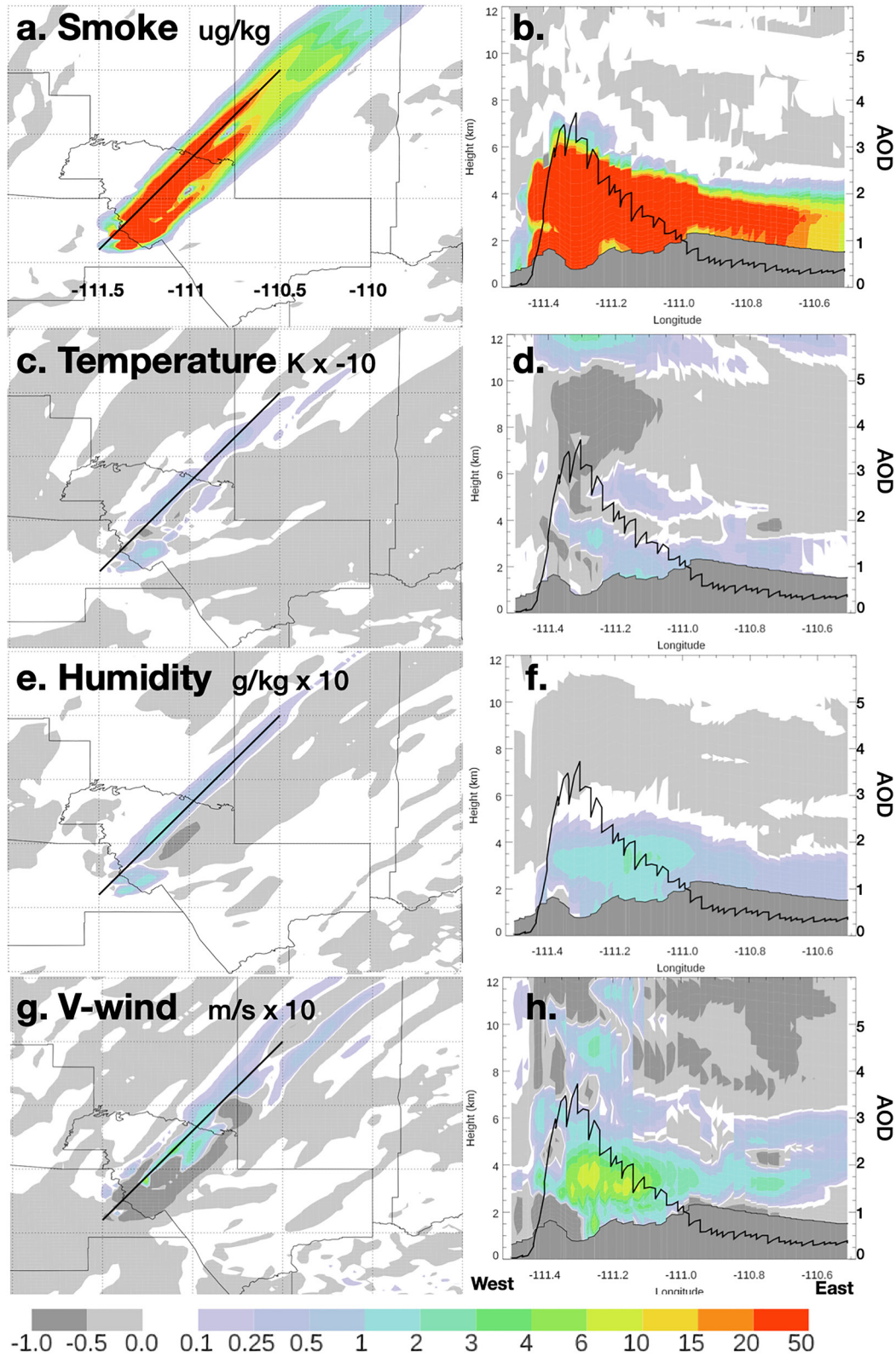

Figure 5. Same as Figure 4, but for the 16 June 2020 case at 2200 UTC.

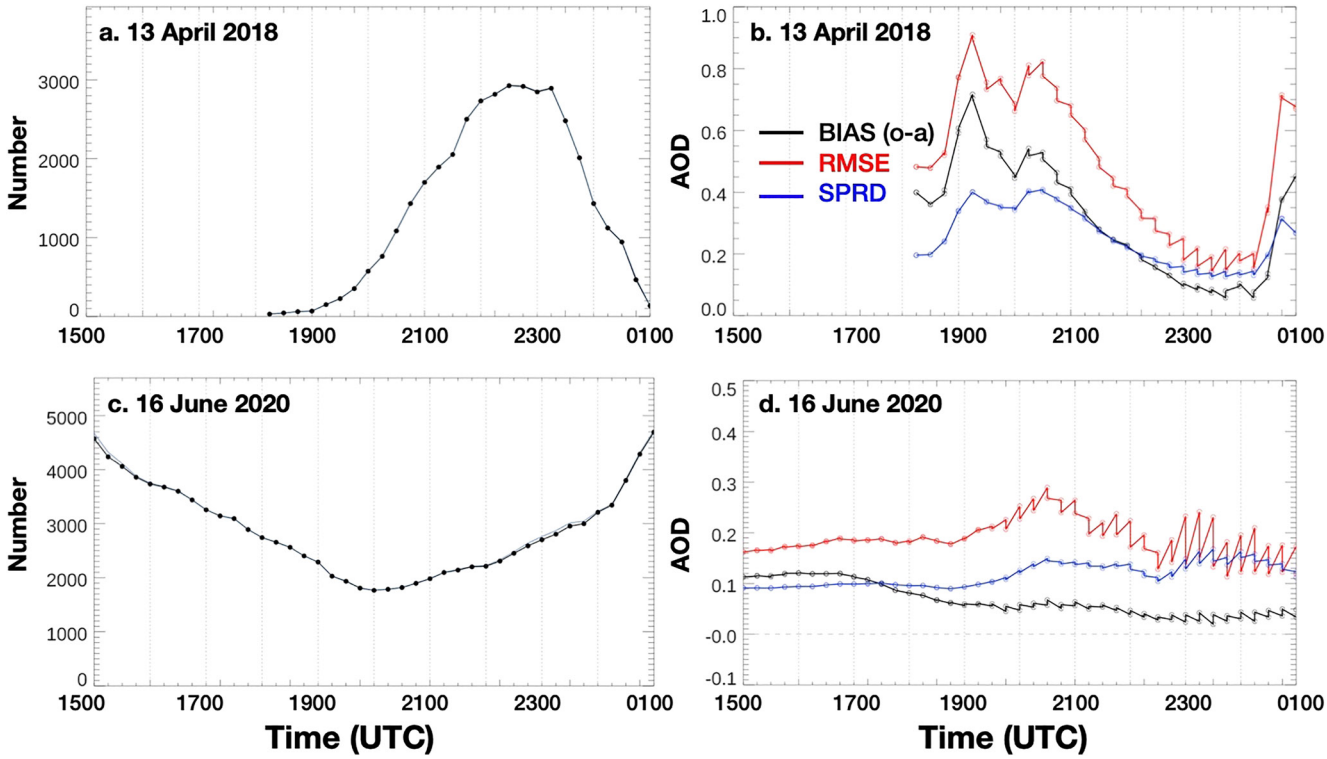

Figure 6. Number of GOES-16 aerosol optical depth retrievals assimilated at each 15 update cycle for the 13 April 2018 (a) and 16 June 2020 (c) cases. Bias (observation—analysis), root mean square error, and total spread (SPRD) at each cycle for each case are provided in panels (b, d).

5. Case Study Results

5.1. 13 April 2018

WoFS-Smoke has the ability to generate probabilistic forecasts of smoke, which are shown here as the probability of total column smoke greater than 50 mg m^{-2}. Smoke forecasts initiated at 2100 UTC are provided in Figure 7 at 45 and 90 min forecast times for both CNTL and WAOD experiments. The forecast differences after 90 min are generally small for this case and all forecast initialization times between 1900–2200 UTC (not shown). Both experiments forecast high probabilities of thick smoke over much of northwestern OK. Smoke plumes from individual fires combine into a single larger plume that extends northeast into Kansas. The coverage of the forecast smoke plume in both experiments increases as a function of forecast time as does the amount of smoke observed. However, significant differences between the smoke forecasts and observations exist. Both experiments fail to forecast the eastward extent of the smoke into central OK and do not clear out the smoke in western OK rapidly enough. Assimilating AOD does produce small, but consistent improvements to the forecast. Smoke probabilities forecast by WAOD are somewhat reduced on the western side of the plume at the analysis time and out to 90 min. Similarly, the eastward extent of the smoke plume is greater in WAOD.

Both trends are apparent when comparing forecast ensemble mean AOD at 2145 UTC (Figure 8). For this time, cross-sections of smoke concentration are calculated along with the corresponding forecast AOD at two different locations. The first (1) represents a west-to-east slice across the primary smoke plume in northern OK (Figures 8c and 8d). The second (2) represents a southwest-to-northeast slice across the leading edge of the smoke plume (Figures 8e and 8f). Also shown are the GOES-16 AOD retrievals along the same path at this time. For cross-section "1," both experiments over-forecast the western extent of the smoke and place the highest smoke concentrations in the same location. CNTL under-forecasts smoke further east, while observed AOD remains greater than 0.5 (Figure 8c). WAOD differs in that the smoke is forecast to extend further east with forecast and GOES-16 AOD in much better agreement (Figure 8d). In the region of maximum smoke concentrations, forecast AOD is much higher than observed, but this is due to limitations in the AOD retrieval algorithm for extreme

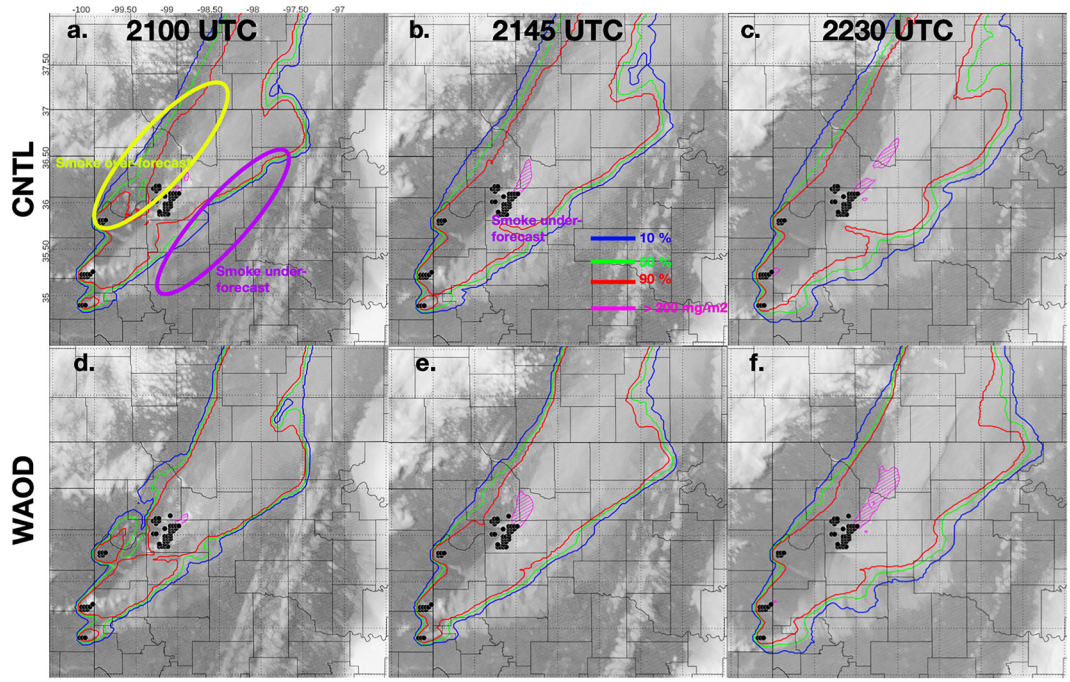

Figure 7. The probability of vertically integrated 2.5 μm diameter particulate matter (PM2.5) > 50 mg m^{-2} contours at 10% (blue), 50% (green) and 90% (red) overlaid on GOES-16 visible imagery valid 2100, 2145, and 2230 UTC 13 April for the CNTL (a–c) and WAOD (d–f) experiments. Also overlaid in pink is the area where the standard deviation of vertically integrated smoke over each ensemble member for the same forecast times is >200 mg m^{-2}. Black dots indicate the locations of model analyzed hotspots at 2100 UTC. Yellow and purple ovals indicate where CNTL under and over-forecasts smoke compared to satellite imagery at 2100 UTC.

aerosol concentrations. Cross-section "2" also indicates that WAOD extends the forecast of smoke further east compared to CNTL (Figures 8e and 8f).

To assess how these differences affect the environment, forecast ensemble mean downward shortwave flux (SWDOWN) at 2145 UTC from both experiments are compared (Figures 9a–9c). Several differences in the SWDOWN forecasts are present and correspond to the eastward shift of the smoke plume apparent in the probabilistic forecast. The difference (WAOD—CNTL) between SWDOWN at 2145 UTC highlights the impact of assimilating AOD (Figure 9a). Overall, more solar radiation is reaching the surface on the west side of the plume in the WAOD experiment compared to the CNTL experiment. A corresponding decrease also exists on the east side. Recall that assimilating AOD should also have impacts on the surrounding environment. To assess these impacts, differences in 2-m temperature, 2-m water vapor mixing ratio, and 10-m meridional wind are also calculated (Figures 9b–9d). In the region between stations WATO and FAIR, the reduction in SWDOWN corresponds to cooling (1°C) and moistening (2 g kg^{-1}) at the surface. Further downstream, the opposite signal is present. Differences in 10 m meridional wind are also apparent, but the overall pattern is less clear. Similar results are present for zonal wind (not shown). One question that arises from this result is whether or not the improvement in AOD forecasts is primary due to the direct assimilation of AOD improving the smoke initial conditions or indirect impacts on the environment, specifically wind. A higher eastward wind speeds would act to transport smoke from west to east more rapidly. However, when comparing wind speed between the experiments in the 0–3 km layer, they were found to be generally small (<2 ms^{-1}). Thus, it appears the improvement in smoke forecasts is largely due to the AOD assimilation correcting biases in the smoke injection due to the poor temporal frequency of the FRP data.

The dense network of surface observation sites provided by the Oklahoma Mesonet creates a rare opportunity to verify the impact on solar radiation from forecast smoke against actual observations. This mesonet is a dense network of surface observation sites that measure temperature, humidity, pressure, wind, and radiation every 5 min within the state of Oklahoma. Figure 10 shows ensemble mean bias (Model—Observation) of SWDOWN at six mesonet sites within the smoke plume for 0–90 min forecasts initiated at 2100 UTC. For sites located near

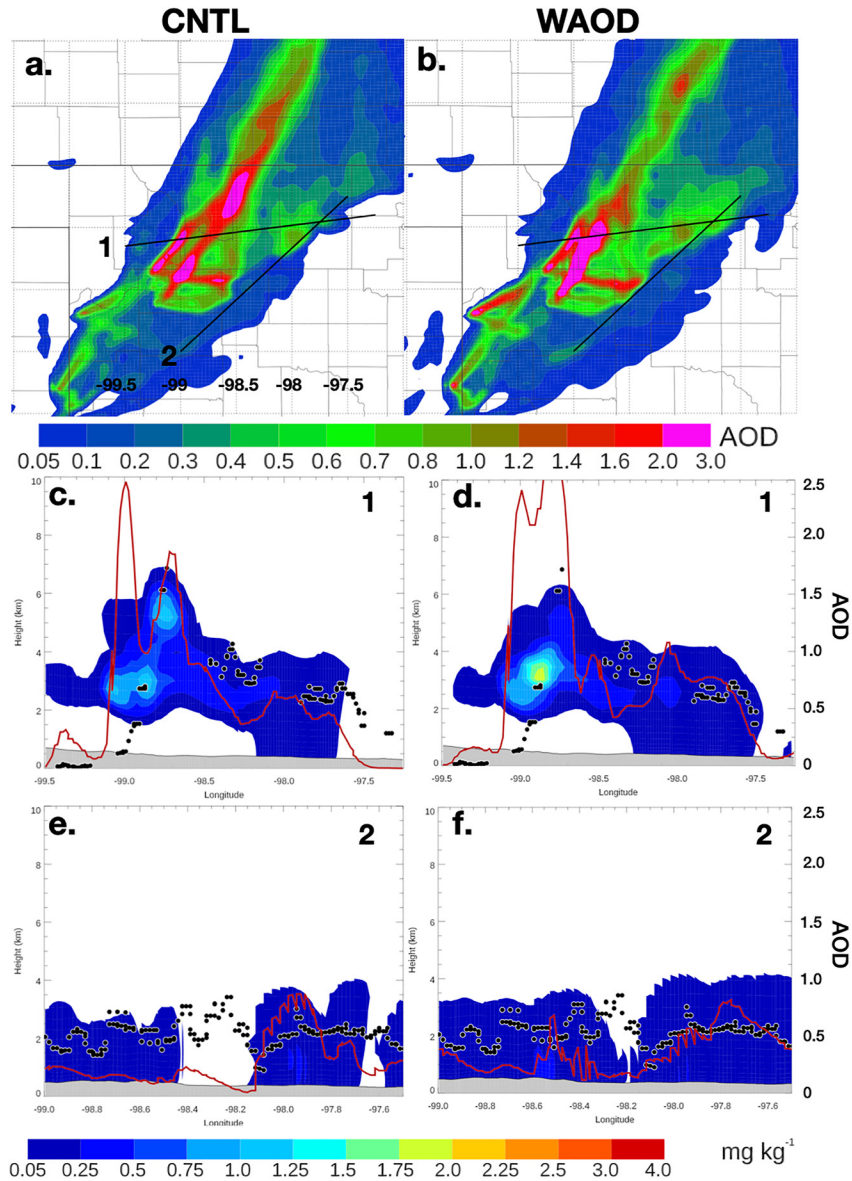

Figure 8. Ensemble mean aerosol optical depth (AOD) at 2145 UTC from a forecast initiated at 2100 UTC 13 April 2018 for CNTL (a) and WAOD (b) experiments. For two cross-sections along the smoke plume, the vertical profile of smoke aerosol concentration (contours), forecast AOD (red line), and observed GOES-16 AOD (black dots) are provided.

the western edge of the smoke plume (FREE, WOOD), CNTL under-forecasts SWDOWN (i.e., over-forecasts smoke) compared to observations between the 15 and 90 min forecast period. Conversely, WAOD generates much lower SWDOWN forecast biases over the same period. This is consistent with the main smoke plume being shifted eastward from assimilating AOD. Forecasts differences between CNTL and WAOD are also apparent in at two sites located within thicker portions of the smoke plume (ALV2, FAIR). For ALV2, there is a small decrease in the 0–60 min forecast bias. However, SWDOWN forecasts at FAIR are not improved in WAOD. After the first 30 min, WAOD over-forecasts SWDOWN (under forecasts smoke) compared to CNTL. It should also be noted that both experiments substantially over-forecast SWDOWN at this site. SWDOWN bias characteristics from sites such as SEIL and PUTN that lie under the heaviest smoke did not differ significantly between experiments (not shown). Given the lower number of AOD retrievals assimilated in these regions, differences were expected to be small. Finally, forecasts at two sites along the eastern side of the smoke plume are compared (LAHO and WATO). At both sites, WAOD generates lower biases due to forecasting more smoke than CNTL, which is consistent with greater eastward extent of the smoke plume in observations compared to the overall

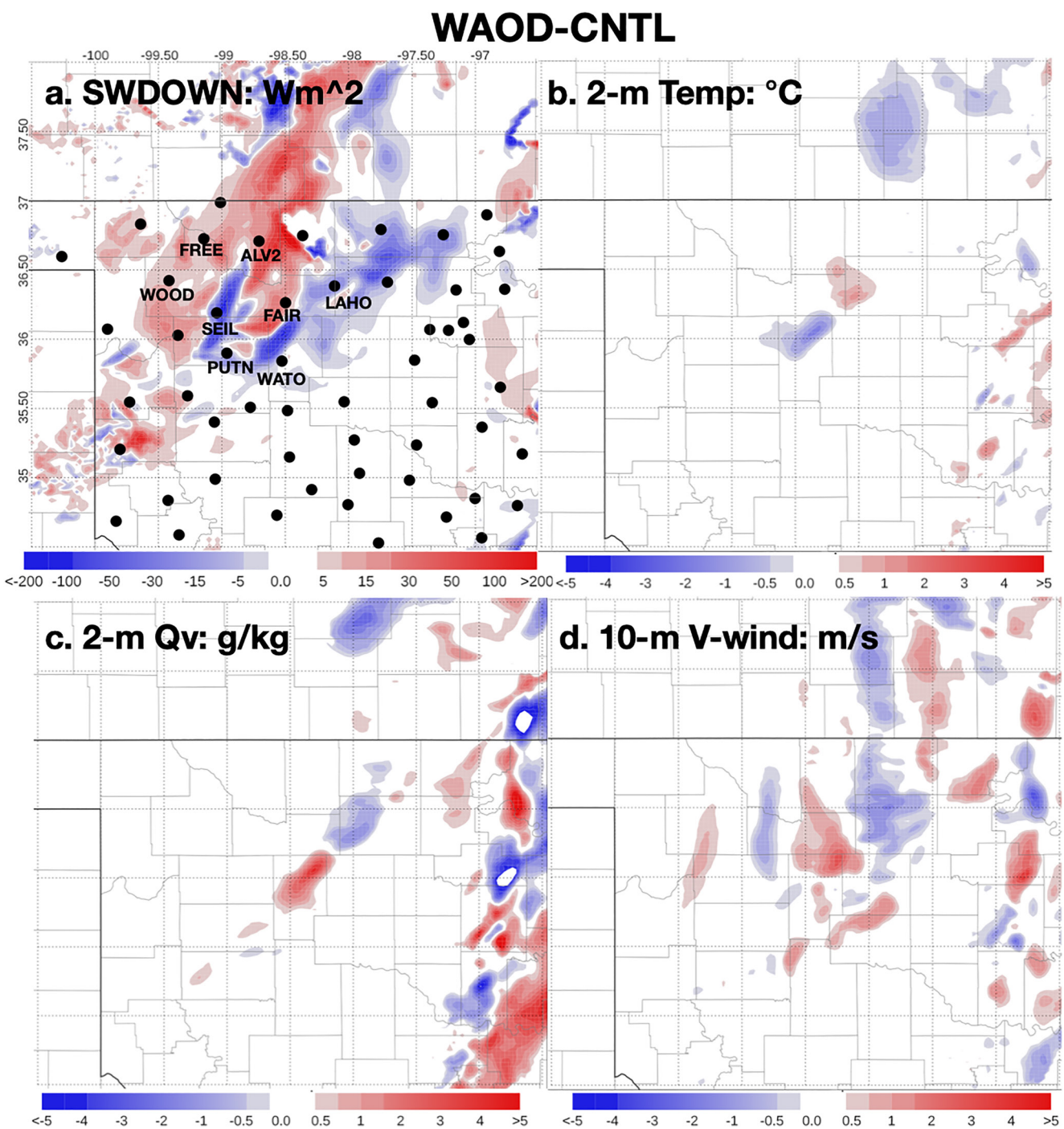

Figure 9. Differences (WAOD-CNTL) between ensemble mean downward shortwave flux (a), 2-m temperature (b), 2-m water vapor mixing ratio (c), and 10-m meridional wind speed (d) 45 min forecasts initiated at 2100 UTC and valid at 2145 UTC 13 April 2018 The locations and names of OK Mesonet stations are overlaid on panel (a).

model forecasts. Verification against other surface observations such as temperature, humidity, and wind speed showed little difference between the experiments. In particular, the difference in wind speed biase between each experiment rarely exceeded 1 ms^{-1}. Results are similar for forecasts initiated at 2000 and 2200 UTC (not shown).

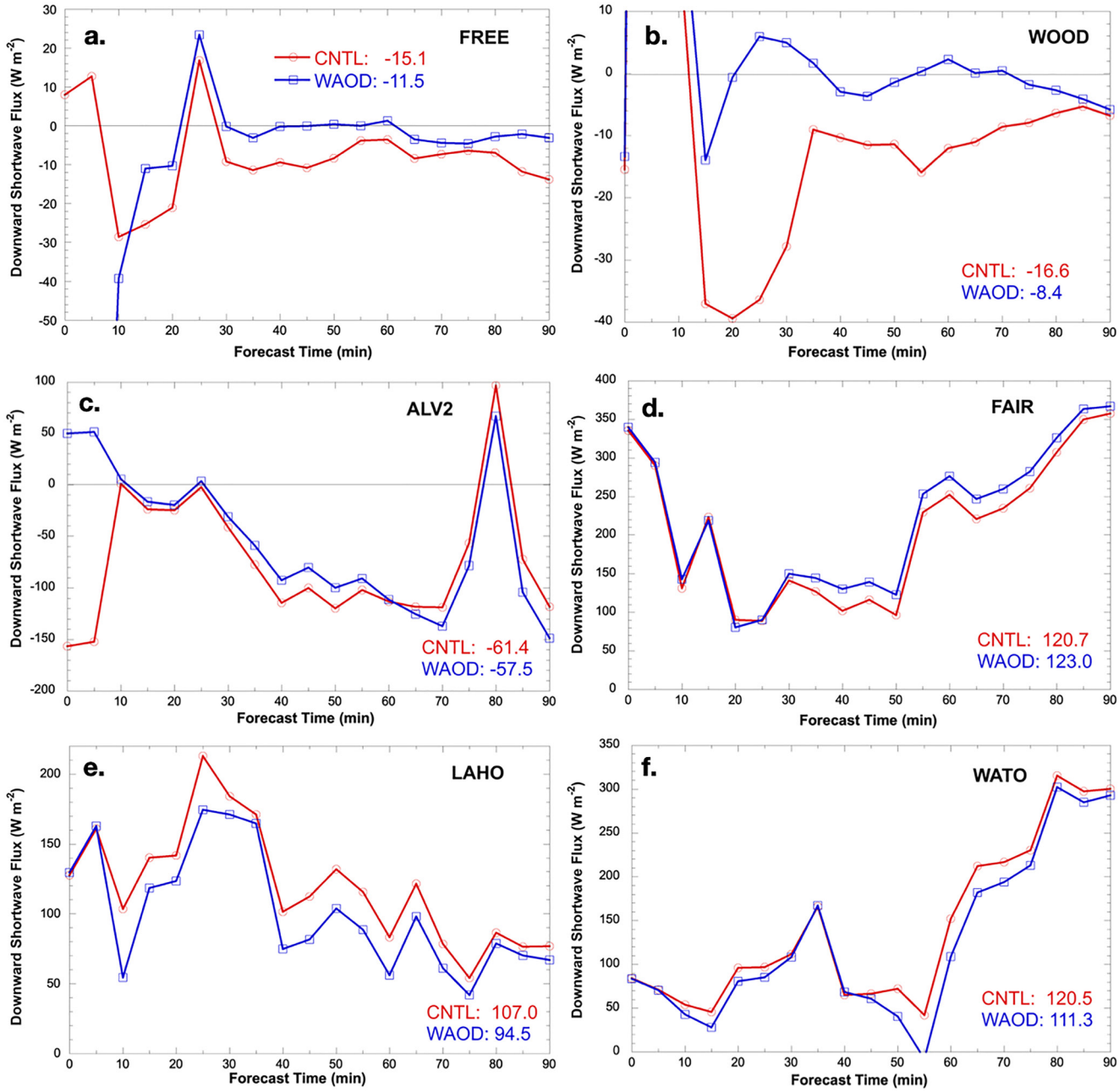

Figure 10. Bias (Model—Observations) of ensemble mean downward shortwave flux (SWDOWN) forecasts initiated at 2100 UTC 13 April for CNTL (red) and WAOD (blue) experiments at six OK Mesonet sites (see Figure 9 for site locations). Positive values indicate WoFS-Smoke is over-forecasting SWDOWN (under-forecasting smoke) and negative values indicate WoFS-Smoke is under-forecasting SWDOWN (over-forecasting smoke). Note that the *y*-axis scales differ from site to site. Average bias between 5 and 90 min forecast time for both experiments are provided for each site.

5.2. 16 June 2020

As with the 13 April 2018 case, probabilistic forecasts of smoke greater than 50 mg m^{-2} are created, but for a 3 hr forecast initiated at 2200 UTC on 16 June 2020. This case was also discussed in Jones et al. (2022) as part of the initial WoFS-Smoke development. Both CNTL and WAOD experiments generated high probability smoke forecasts emanating from the two major fires in AZ for the entire 3 hr forecast period (Figure 11). Assimilating GOES-16 AOD retrievals results in forecast smoke probability contours better matching the outline of the smoke plume observed in visible data at 2200 UTC (Figures 11a and 11d). These differences remain at later forecast times, but are confined to the downstream portion of the smoke plume. In addition to plume shape, the amount

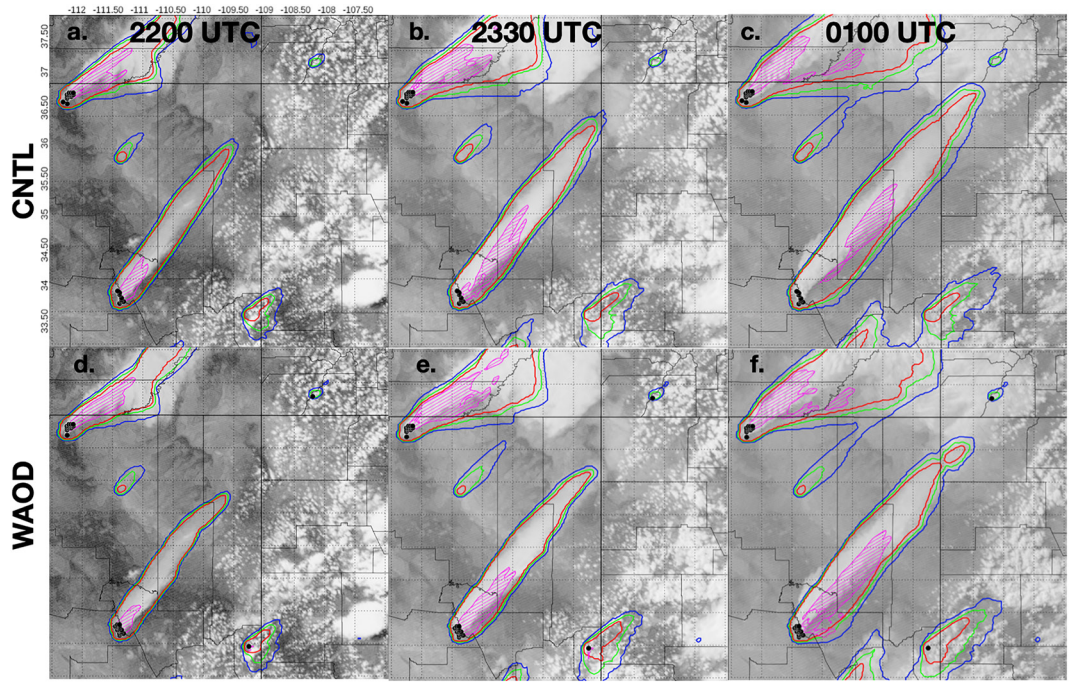

Figure 11. Same as Figure 7, but for 0, 90, and 180 min forecasts initiated at 2200 UTC 16 June 2020.

of smoke forecast is also noticeability different between the two experiments. In the downstream portion of the plume, WAOD forecasts lower smoke concentrations compared to the CNTL. Both experiments over-forecast the southeastward extent of the main smoke plume and assimilating AOD only marginally improves this portion of the forecast. Corresponding forecast AOD is also much lower in the WAOD experiment at 2330 UTC in the downstream portion of the smoke plume (Figures 12a and 12b). Smoke forecasts associated with the Mangum fire are similar from a probabilistic perspective for both experiments.

Cross-sections were computed across the Bush fire smoke plume at two different locations, this time for 90 min forecasts valid at 2330 UTC 16 June 2020 (Figure 12). The first cross-section (1), is a northwest-to-southwest slice across the plume where forecast AOD exceeds 5.0 in CNTL (Figure 12c). Both smoke and AOD forecasts show the relatively narrow, but high concentration smoke plume at this time. The eastward bias in the forecast smoke plume is also evident when compared against GOES-16 retrievals. WAOD differs in several aspects (Figure 12d). First, forecast smoke concentrations are much lower, but also extend somewhat further west. Forecast AOD and GOES-16 AOD retrievals are in much better agreement, but recall that AOD retrievals in the heart of the smoke plume may be underestimates. A second cross section (2) further northeast show much lower forecast smoke concentrations in both experiments (Figures 12e and 12f). At this location, CNTL over-forecasts AOD while WAOD under-forecasts AOD. These differences are consistent with the differences upstream in cross section "1".

The difference in ensemble mean downward shortwave flux at 2330 UTC from both experiments shows the location of both primary smoke plumes (Figure 13a). A decrease over 500 Wm^{-2} in solar radiation reaching the surface exists between the environment and the thickest portion of the smoke plumes. The forecasted decrease with the Bush fire is less in WAOD, corresponding to the lower smoke concentrations forecast downstream (Figure 13a). However, near the origin WAOD actually increases smoke aerosol concentrations, leading to less solar radiation reaching the surface. Overall, the forecast smoke plume associated with the Bush fire is shifted slightly east and is weaker at most locations downstream of the origin. Other differences between CNTL and WAOD forecasts are present with the Mangum fire smoke plume. The magnitude of the differences is smaller, but WAOD forecasts lower smoke concentrations southeast of the main smoke plume leading to more solar radiation reaching the surface. Conversely, WAOD forecasts higher smoker concentrations (less solar radiation reaching the surface) along the path where both experiments have the most intense portion of the plume. Additional differences occur when comparing forecasts of the surrounding environment. The decrease in forecast smoke by WAOD results in an increase in 2-m temperature of 1–2°C over a large area (Figure 13b). However, 2-m water

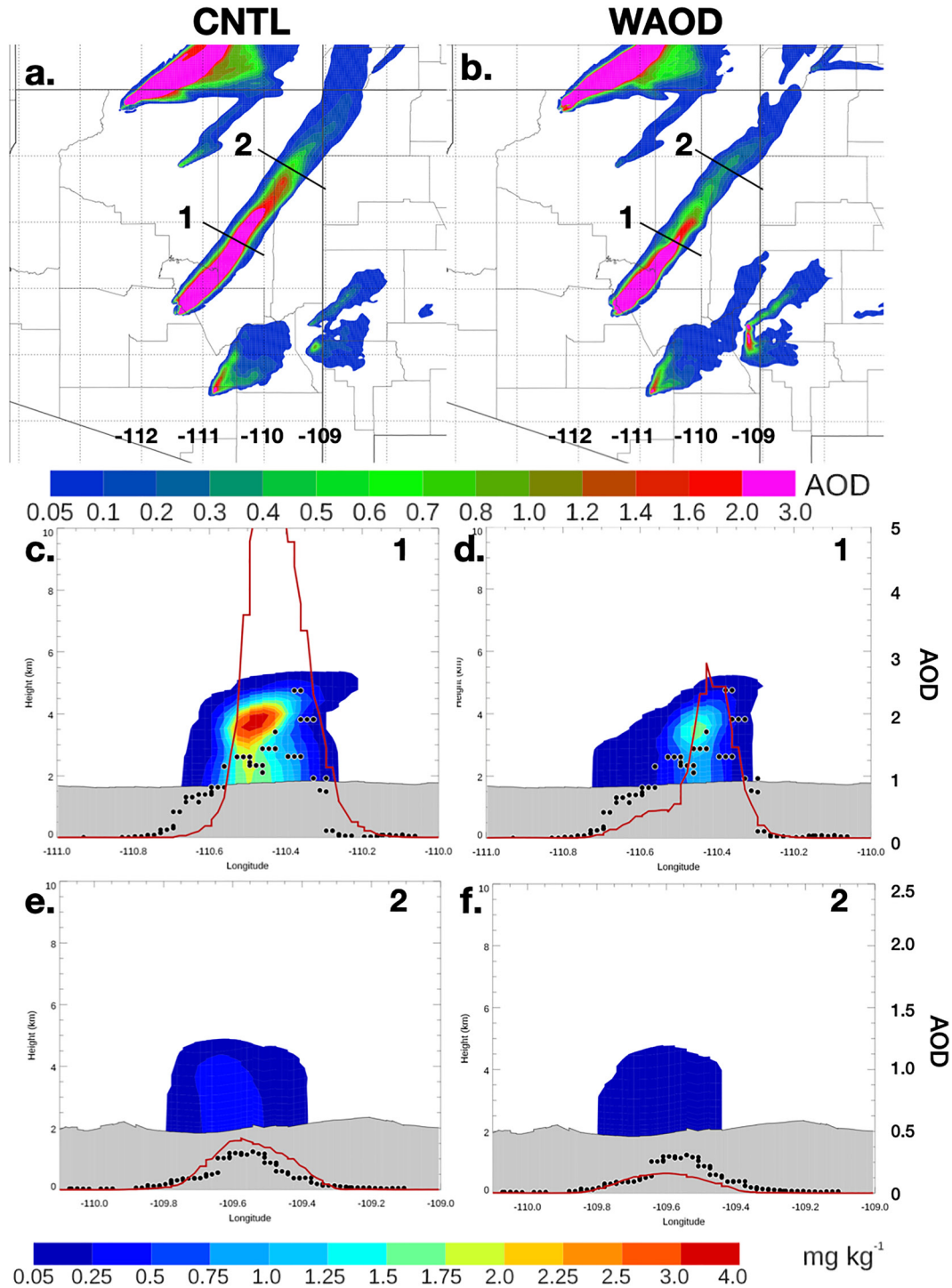

Figure 12. Same as Figure 8, but at 2330 UTC from a forecast initiated at 2200 UTC 16 June 2020.

vapor mixing ratio also decreases, with WAOD forecasting slightly drier conditions (Figure 13c). This result differs from the 13 April case and the covariance analysis conducted for both cases where moistening is expected. However, the maximum moistening signal is 2–4 km above the surface and the 2-m difference plotted here does not capture the increasing moisture at higher levels. Plots at higher levels do show that WAOD forecasts greater moisture content at these levels as expected (not shown). Finally, differences in forecast 10-m meridional wind speed are generally confined to the edges of the smoke plume (Figure 13d). Unfortunately, these smoke plumes

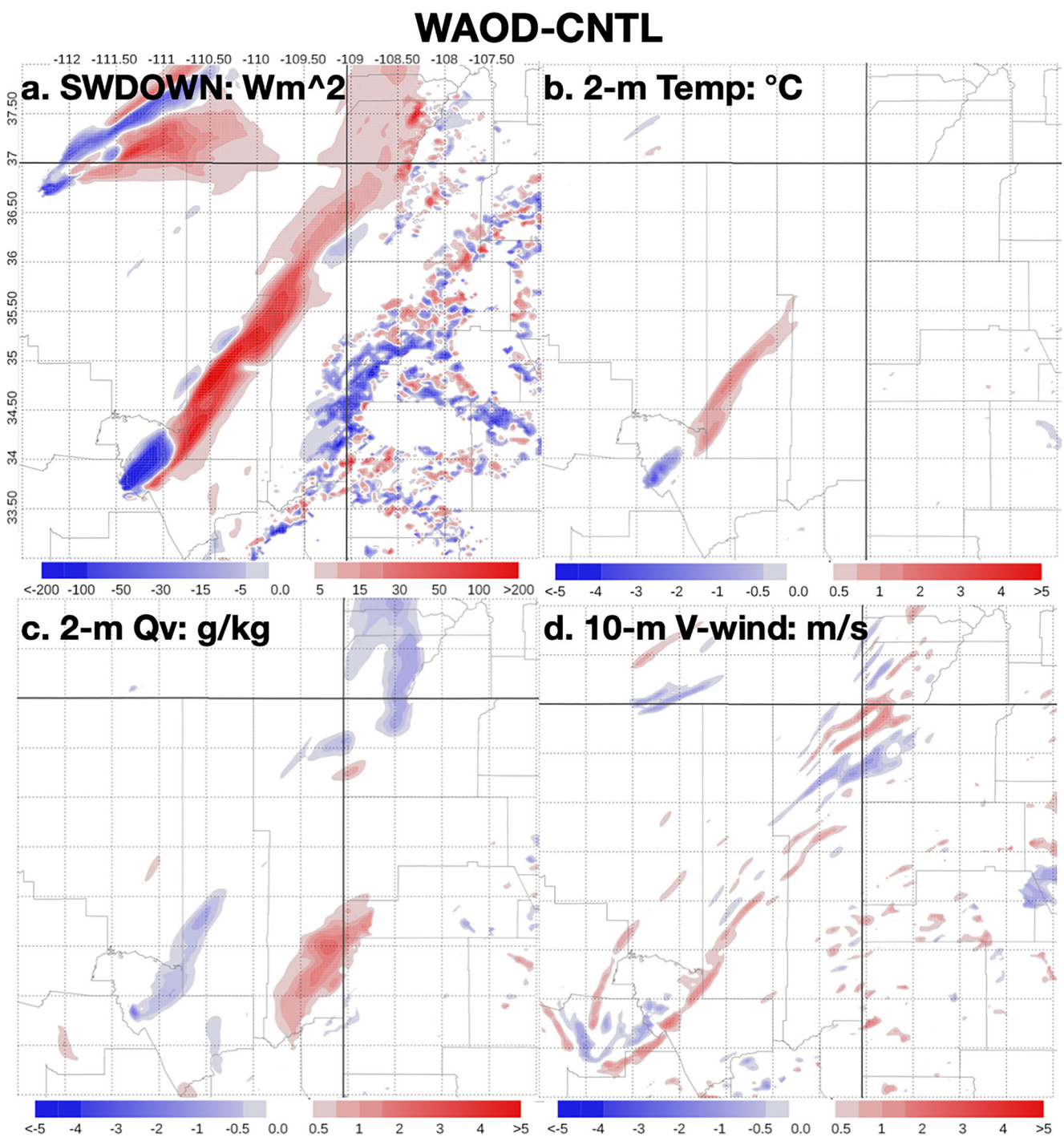

Figure 13. Same as Figure 9, but for a 90 min forecast initiated at 2200 UTC 16 June 2020 and valid at 2330 UTC.

did not pass over any surface observation sites for which data were available, preventing a full qualitative assessment of the smoke forecasts for this case.

6. Conclusions

Incorporating an AOD assimilation capability into WoFS-Smoke had the desired effect of modifying the analyses smoke aerosol concentrations sometimes leading to improved 0–3 hr forecasts of smoke and incoming solar radiation. Comparing the relationship between 2-D AOD and 3-D atmospheric variables indicates that assimilating AOD not only directly affects smoke aerosol concentrations, but also has indirect impacts to temperature, humidity, and wind. AOD is positively correlated with smoke and often negatively correlated with temperature. Larger AOD sometimes corresponds to an increase in forecast atmospheric moisture, which is a result that will be explored further. Additional correlations with wind speed and direction are present especially along the smoke plume edges.

The number and characteristics of AOD retrievals change significantly due to changing wildfire conditions. These changes result in the optimization of the AOD assimilation also changing as a function of time. The optimization is maximized where observed AOD from smoke lies between 0.25 and 1.0. These areas generally correspond to the downstream portions of the smoke plumes away from the source fire. Where smoke concentrations are greatest near the wildfire origin, valid AOD retrievals are often not made due to being miss-classified as clouds. This can severely limit the impact of AOD assimilation and improved GOES-R AOD retrievals in these regions would be greatly beneficial. For low concentrations of smoke aerosols generated by previous fires, the difference between retrievals and the model analyses are generally small leading to only minor impacts from assimilation in these areas.

For the 13 April 2018 case, assimilating AOD adjusts the smoke plume eastward, partially correcting the west bias in the forecast smoke plume when not assimilating AOD data. The positive impact is generally only present for the first 90 min of the forecast when verified against both satellite and surface observations. The direct impact of the AOD assimilation rather than indirect impacts to other atmospheric variables such as wind appears to be the main factor in the observed improvement. However, the magnitude of the improvement is small in some circumstances indicating further room for improvement in the system. Assimilating AOD also had a substantial impact on smoke forecasts of the 16 June 2020 case. Verification of this case is more difficult given the lack of surface observations and potential biases in the AOD retrievals. WAOD also generated 0–3 hr AOD forecasts that better matched the retrievals, but there is evidence that the retrievals are negatively biased. Thus, actual smoke concentrations may be under-forecast.

Despite the generally positive results, there are many aspects of AOD assimilation into WoFS-Smoke that require further research. Future work will utilize a RTM forward operator in place of the more simplistic approach applied here. The importance of biases in both retrievals and the model will also be further examined. These biases are likely one of the reasons for the less than optimal results seen in portions of these experiments. In addition, future experiments will conduct verification with surface air quality measurements, which were not available here.

Finally, future versions of WoFS-Smoke will implement further linkages between aerosol and cloud properties (Conrick et al., 2021; Grell et al., 2011), so that assimilating AOD can directly impact analyzed cloud and precipitation features.

Data Availability Statement

The WoFS-Smoke output used generated for these and additional experiments are available at https://wof.nssl.noaa.gov/. The data assimilation code and forecast data used to generate these results are available at https://doi.org/10.5281/zenodo.7190820 and the NSSL anonymous FTP server at ftp.nssl.noaa.gov/projects/warnonforecast/. WoFS model output are generated in netcdf format.

Acknowledgments
This research was funded in part by the NOAA Warn-on-Forecast project. Additional funding was provided the under the NOAA-University of Oklahoma Cooperative Agreement NA21OAR4320204, U.S. Department of Commerce. HRRR ensemble initial and boundary conditions for this work were provided by the Global Systems Laboratory as part of real-time experiments. We also want to thank Dr. Amanda Back for her review of this work.

References

Ahmadov, R., Grell, G., James, E., Csiszar, I., Tsidulko, M., Pierce, B., et al. (2017). Using VIIRS Fire Radiative Power data to simulate biomass burning emissions, plume rise and smoke transport in a real-time air quality modeling system. In *2017 IEEE international symposium on geoscience and remote sensing IGARSS* (pp. 2806–2808). IEEE.

Back, A., Ahmadov, R., James, E. P., Grell, G., Pereira, G., Freitas, S. R., et al. (2020). Use of VIIRS aerosol optical depth information at NOAA GSL to improve smoke, visibility, and weather forecasts in the experimental high resolution rapid refresh. *JCSDA Quarterly Newsletter*, *67*, 1–6. https://doi.org/10.25923/4pt1-wx36

Benedetti, A., Di Giuseppe, F., Jones, L., Peuch, V.-H., Rémy, S., & Zhang, X. (2019). The value of satellite observations in the analysis and short-range prediction of Asian dust. *Atmospheric Chemistry and Physics*, *19*(2), 987–998. https://doi.org/10.5194/acp-19-987-2019

Benedetti, A., Morcrette, J.-J., Boucher, O., Dethof, A., Engelen, R. J., Fisher, M., et al. (2009). Aerosol analysis and forecast in the European Centre for medium-range weather forecasts integrated forecast system: 2. Data assimilation. *Journal of Geophysical Research*, *114*(D13), D13205. https://doi.org/10.1029/2008jd011115

Chen, D., Liu, Z., Davis, C., & Gu, Y. (2017). Dust radiative effects on atmospheric thermodynamics and tropical cyclogenesis over the Atlantic Ocean using WRF-Chem coupled with an AOD data assimilation system. *Atmospheric Chemistry and Physics*, *17*(12), 7917–7939. https://doi.org/10.5194/acp-17-7917-2017

Choi, Y., Chen, S. H., Huang, C. C., Earl, K., Chen, C. Y., Schwartz, C. S., & Matsui, T. (2020). Evaluating the impact of assimilating aerosol optical depth observations on dust forecasts over North Africa and the East Atlantic using different data assimilation methods. *Journal of Advances in Modeling Earth Systems*, *12*(4), e2019MS001890. https://doi.org/10.1029/2019ms001890

Coakley, J. A., Jr., Cess, R. D., & Yurevich, F. B. (1983). The effect of tropospheric aerosols on the Earths radiation budget: A parameterization for climate models. *Journal of the Atmospheric Sciences*, *40*(1), 116–138. https://doi.org/10.1175/1520-0469(1983)040<0116:teotao>2.0.co;2

Conrick, R., Mass, C. F., Boomgard-Zagrodnik, J. P., & Ovens, D. (2021). The influence of wildfire smoke on cloud microphysics during the September 2020 Pacific Northwest wildfires. *Weather and Forecasting*, *36*, 1519–1536.

Dowell, D. C., Alexander, C. R., James, E. P., Weygandt, S. S., Benjamin, S. G., Manikin, G. S., et al. (2022). The High-Resolution Rapid Refresh: An hourly updating convection-allowing forecast model. Part 1: Motivation and system description. *Weather and Forecasting*, *37*(8), 1371–1395. https://doi.org/10.1175/waf-d-21-0151.1

Freitas, S. R., Longo, K. M., & Andreae, M. O. (2006). Impact of including the plume rise of vegetation fires in numerical simulations of associated atmospheric pollutants. *Geophysical Research Letters*, *33*(17), 1–5. https://doi.org/10.1029/2006gl026608

Freitas, S. R., Longo, K. M., Chatfield, R., Latham, D., Dias, M., Andreae, M. O., et al. (2007). Including the sub-grid scale plume rise of vegetation fires in low resolution atmospheric transport models. *Atmospheric Chemistry and Physics*, *7*(13), 3385–3398. https://doi.org/10.5194/acp-7-3385-2007

Fromm, M., Kablick, G., III., & Caffrey, P. (2016). Dust-infused baroclinic cyclone storm clouds: The evidence, meteorology, and some implications. *Geophysical Research Letters*, *43*(24), 12643–12650. https://doi.org/10.1002/2016GL071801

Fromm, M. D., Lindsey, D. T., Servranckx, R., Yue, G., Trickl, T., Sica, R., & Godin-Beekmann, S. (2010). The untold story of pyrocumulonimbus. *Bulletin America Meteorology Social*, *91*(9), 1193–1209. https://doi.org/10.1175/2010bams3004.1

Fromm, M. D., Tupper, A., Rosenfeld, D., Servranckx, R., & McRae, R. (2006). Violent pyro-convective storm devastates Australia's capital and pollutes the stratosphere. *Geophysical Research Letters*, *33*(5), L05815. https://doi.org/10.1029/2005gl025161

Gaspari, G., & Cohn, S. E. (1999). Construction of correlation functions in two and three dimensions. *Quarterly Journal of the Royal Meteorological Society*, *125*(554), 723–757. https://doi.org/10.1002/qj.49712555417

Grell, G., Freitas, S. R., Stuefer, M., & Fast, J. (2011). Inclusion of biomass burning in WRF-Chem: Impact of wildfires on weather forecasts. *Atmospheric Chemistry and Physics*, *11*, 5289–5303. https://doi.org/10.5194/acp-11-5289-2011

Hu, M., Shao, H., Stark, D., Newman, K., Zhou, C., & Zhang, X. (2016). Grid-point statistical interpolation (GSI) user's guide version 3.5. Developmental testbed center (p. 141). Retrieved from http://www.dtcenter.org/com-GSI/users/docs/index.php

Iacono, M. J., Delamere, J. S., Mlawer, E. J., Clough, S. A., Morcrette, J.-J., & Hou, Y.-T. (2004). Development and evaluation of RRTMG_SW, a shortwave radiative transfer model for general circulation model applications. In *Proceedings of the 14th atmospheric radiation measurement (ARM) science team meeting* (p. 10). DOE.

James, E. P., Alexander, C. R., Dowell, D. C., Weygandt, S. S., Benjamin, S. G., Manikin, G. S., et al. (2022). The High-Resolution Rapid Refresh (HRRR): An hourly updating convection-allowing forecast model. Part 2: Forecast performance. *Weather and Forecasting*, *37*(8), 1397–1417. https://doi.org/10.1175/waf-d-21-0130.1

Jones, T. A., Ahmadov, R., James, E., Periria, G., Freitas, S., & Grell, G. (2022). Prototype of a Warn-on-Forecast System for Smoke (WoFS-Smoke). *Weather and Forecasting*, *37*(7), 1191–1209. https://doi.org/10.1175/waf-d-21-0143.1

Jones, T. A., Knopfmeier, K., Wheatley, D., Creager, G., Minnis, P., & Palikonda, R. (2016). Storm- scale data assimilation and ensemble forecasting with the NSSL experimental Warn-on- Forecast system. Part II: Combined radar and satellite data experiments. *Weather and Forecasting*, *31*(1), 297–327. https://doi.org/10.1175/waf-d-15-0107.1

Jones, T. A., Skinner, P., Yussouf, N., Knopfmeier, K., Reinhart, A., Wang, X., et al. (2020). Assimilation of GOES-16 radiances and retrievals into the Warn-on-Forecast System. *Monthly Weather Review*, *148*(5), 1829–1859. https://doi.org/10.1175/mwr-d-19-0379.1

Kaufman, Y. J., Tanre, D., Nakajima, T., Lenoble, J., Frouin, R., Grassl, H., et al. (1997). Passive remote sensing of tropospheric aerosol and atmospheric correction for the aerosol effect. *Journal of Geophysical Research*, *102*(D14), 16815–16830. https://doi.org/10.1029/97jd01496

Kleist, D. T., Parrish, D. F., Derber, J. C., Treadon, R., Wu, W.-S., & Lord, S. (2009). Introduction of the GSI into the NCEP global data assimilation system. *Weather and Forecasting*, *24*(6), 1691–1705. https://doi.org/10.1175/2009waf2222201.1

Kochanski, A., Mallia, D. V., Fearon, M., Brown, T., Souri, A. H., & Mandel, J. (2019). Modeling wildfire smoke feedback mechanisms using a coupled fire-atmosphere model with a radiatively active aerosol scheme. *Journal of Geophysical Research: Atmospheres*, *124*(16), 9099–9116. https://doi.org/10.1029/2019jd030558

Koren, I., Remer, L. A., Kaufman, Y. J., Rudich, Y., & Martins, J. V. (2007). On the twilight zone between clouds and aerosols. *Geophysical Research Letters*, *34*(8), L08805. https://doi.org/10.1029/2007gl029253

Lareau, N. P., & Clements, C. B. (2015). Cold smoke: Smoke-induced density currents cause unexpected smoke transport near large wildfires. *Atmospheric Chemistry and Physics*, *15*(20), 11513–11520. https://doi.org/10.5194/acp-15-11513-2015

Levy, R. C., Remer, L. A., Mattoo, S., Vermote, E. F., & Kaufman, Y. J. (2007). Second- generation operational algorithm: Retrieval of aerosol properties over land from inversion of Moderate Resolution Imaging Spectroradiometer spectral reflectance. *Journal of Geophysical Research*, *112*(D13), D13211. https://doi.org/10.1029/2006JD007811

Liu, Z., Liu, Q., Lin, H.-C., Schwartz, C. S., Lee, Y.-H., & Wang, T. (2011). Three-dimensional variational assimilation of MODIS aerosol optical depth: Implementation and application to a dust storm over East Asia. *Journal of Geophysical Research*, *116*(D23), D23206. https://doi.org/10.1029/2011jd016159

Mann, G. W., Carslaw, K. S., Reddington, C. L., Pringle, K. J., Schulz, M., Asmi, A., et al. (2014). Intercomparison and evaluation of global aerosol microphysical properties among AeroCom models of a range of complexity. *Atmospheric Chemistry and Physics*, *14*(9), 4679–4713. https://doi.org/10.5194/acp-14-4679-2014

Mlawer, E. J., Taubman, S. J., Brown, P. D., Iacono, M. J., & Clough, S. A. (1997). Radiative transfer for inhomogeneous atmospheres: RRTM, a validated correlated-k model for the longwave. *Journal of Geophysical Research*, *102*(D14), 16663–16682. https://doi.org/10.1029/97JD00237

Pandolfi, M., Tobias, A., Alastuey, A., Sunyer, J., Schwartz, J., Lorente, J., et al. (2014). Effect of atmospheric mixing layer depth variations on urban air quality and daily mortality during Saharan dust outbreaks. *Science of the Total Environment*, *494–495*, 283–289. https://doi.org/10.1016/j.scitotenv.2014.07.004

Peng, Z., Liu, Z., Chen, D., & Ban, J. (2017). Improving PM2.5 forecast over China by the joint adjustment of initial conditions and source emissions with an ensemble Kalman filter. *Atmospheric Chemistry and Physics*, *17*(7), 4837–4855. https://doi.org/10.5194/acp-17-4837-2017

Pope, C. A., III., Burnett, R. T., Thun, M. J., Calle, E. E., Krewski, D., Ito, K., & Thurston, G. D. (2002). Lung cancer, cardiopulmonary mortality, and long-term exposure to fine particulate air pollution. *JAMA*, *287*(9), 1132–1141. https://doi.org/10.1001/jama.287.9.1132

Powers, J. G., Klemp, J. B., Skamarock, W. C., Davis, C. A., Dudhia, J., Gill, D. O., et al. (2017). The weather research and forecasting model overview, system efforts, and future directions. *Bulletin America Meteorology Social*, *98*(8), 1717–1737. https://doi.org/10.1175/bams-d-15-00308.1

Randles, C. A., da Silva, A. M., Buchard, V., Colarco, P. R., Darmenov, A., Govindaraju, R., et al. (2017). The MERRA-2 aerosol reanalysis, 1980 onward. Part I: System description and data assimilation evaluation. *Journal of Climate*, *30*(17), 6823–6850. https://doi.org/10.1175/jcli-d-16-0609.1

Remer, A., Kaufman, Y. J., Tanre, D., Mattoo, S., Chu, D. A., Martins, J. V., et al. (2005). The MODIS aerosol algorithm, products, and validation. *Journal of the Atmospheric Sciences*, *62*(4), 947–973. https://doi.org/10.1175/jas3385.1

Robock, A. (1988). Enhancement of surface cooling due to forest fire smoke. *Science*, *242*(4880), 911–913. https://doi.org/10.1126/science.242.4880.911

Robock, A. (1991). Surface cooling due to forest fire smoke. *Journal of Geophysical Research*, *96*(D11), 20869. https://doi.org/10.1029/91jd02043

Rubin, J. I., Reid, J. S., Hansen, J. A., Anderson, J. L., Collins, N., Hoar, T. J., et al. (2016). Development of the Ensemble Navy Aerosol Analysis Prediction System (ENAAPS) and its application of the Data Assimilation Research Testbed (DART) in support of aerosol forecasting. *Atmospheric Chemistry and Physics*, *16*(6), 3927–3951. https://doi.org/10.5194/acp-16-3927-2016

Rubin, J. I., Reid, J. S., Hansen, J. A., Anderson, J. L., Holben, B. N., Xian, P., et al. (2017). Assimilation of AERONET and MODIS AOT observations using variational and ensemble data assimilation methods and its impact on aerosol forecasting skill. *Journal of Geophysical Research: Atmospheres*, *122*(9), 4967–4992. https://doi.org/10.1002/2016jd026067

Saide, P. E., Carmichael, G. R., Liu, Z., Schwartz, C. S., Lin, H. C., da Silva, A. M., & Hyer, E. (2013). Aerosol optical depth assimilation for a size-resolved sectional model: Impacts of observationally constrained, multi-wavelength and fine mode retrievals on regional scale analyses and forecasts. *Atmospheric Chemistry and Physics*, *13*(20), 10425–10444. https://doi.org/10.5194/acp-13-10425-2013

Saide, P. E., Kim, J., Song, C. H., Choi, M., Cheng, Y., & Carmichael, G. R. (2014). Assimilation of next generation geostationary aerosol optical depth retrievals to improve air quality simulations. *Geophysical Research Letters*, *41*(24), 9188–9196. https://doi.org/10.1002/2014gl062089

Schwartz, C. S., Romine, G. S., Smith, K. R., & Weisman, M. L. (2014). Characterizing and optimizing precipitation forecasts from a convection-permitting ensemble initialized by a mesoscale ensemble Kalman filter. *Weather and Forecasting*, *29*(6), 1295–1318. https://doi.org/10.1175/waf-d-13-00145.1

Sekiyama, T. T., Tanaka, T. Y., Shimizu, A., & Miyoshi, T. (2010). Data assimilation of CALIPSO aerosol observations. *Atmospheric Chemistry and Physics*, *10*(1), 39–49. https://doi.org/10.5194/acp-10-39-2010

Skamarock, W. C., Klemp, J. B., Dudhia, J., Gill, D. O., Barker, D., Duda, M. G., et al. (2008). *A description of the advanced research WRF version 3* (p. 113). NCAR Tech. Note NCAR/TN-4751STR.

Skinner, P. S., Wheatley, D. M., Knopfmeier, K. H., Reinhart, A. E., Choate, J. J., Jones, T. A., et al. (2018). Object-based verification of a prototype Warn-on-Forecast system. *Weather and Forecasting*, *33*(5), 1225–1250. https://doi.org/10.1175/waf-d-18-0020.1

Stensrud, D. J., Wicker, L. J., Xue, M., Dawson, D. T., Yussouf, N., Wheatley, D. M., et al. (2013). Progress and challenges with Warn-on-Forecast. *Atmospheric Research*, *123*, 2–16. https://doi.org/10.1016/j.atmosres.2012.04.004

Stensrud, D. J., Xue, M., Wicker, L. J., Kelleher, K. E., Foster, M. P., Schaefer, J. T., et al. (2009). Convective-scale Warn-on-Forecast system: A vision for 2020. *Bulletin America Meteorology Social*, *90*(10), 1487–1499. https://doi.org/10.1175/2009bams2795.1

Textor, C., Schulz, M., Guibert, S., Kinne, S., Balkanski, Y., Bauer, S., et al. (2006). Analysis and quantification of the diversities of aerosol life cycles within AeroCom. *Atmospheric Chemistry and Physics*, *6*(7), 1777–1813. https://doi.org/10.5194/acp-6-1777-2006

Textor, C., Schulz, M., Guibert, S., Kinne, S., Balkanski, Y., Bauer, S., et al. (2007). The effect of harmonized emissions on aerosol properties in global models—An AeroCom experiment. *Atmospheric Chemistry and Physics*, *7*(17), 4489–4501. https://doi.org/10.5194/acp-7-4489-2007

Tsikerdekis, A., Schutgens, N. A. J., & Hasekamp, O. P. (2020). Assimilating aerosol optical properties related to size and absorption from POLDER/PARASOL with an ensemble data assimilation system. *Atmospheric Chemistry and Physics Discussions*. https://doi.org/10.5194/acp-2020-468

Twomey, S. A. (1977). The influence of pollution on the shortwave albedo of clouds. *Journal of the Atmospheric Sciences*, *34*(7), 1149–1152. https://doi.org/10.1175/1520-0469(1977)034<1149:tiopot>2.0.co;2

Wheatley, D. M., Knopfmeier, K. H., Jones, T. A., & Creager, G. J. (2015). Storm-scale data assimilation and ensemble forecasting with the NSSL Experimental Warn-on-Forecast System. Part I: Radar data experiments. *Weather and Forecasting*, *30*(6), 1795–1817. https://doi.org/10.1175/waf-d-15-0043.1

Whitaker, J. S., Hamill, T. M., Wei, X., Song, Y., & Toth, Z. (2008). Ensemble data assimilation with the NCEP Global Forecast System. *Monthly Weather Review*, *136*(2), 463–482. https://doi.org/10.1175/2007MWR2018.1

Yumimoto, K., Nagao, T. M., Kikuchi, M., Sekiyama, T. T., Murakami, H., Tanaka, T. Y., et al. (2016). Aerosol data assimilation using data from Himawari-8, a next-generation geostationary meteorological satellite. *Geophysical Research Letters*, *43*(11), 5886–5894. https://doi.org/10.1002/2016gl069298

Yussouf, N., & Knopfmeier, K. H. (2019). Application of Warn-on-Forecast System for flash- flood producing heavy convective rainfall events. *Quarterly Journal of the Royal Meteorological Society*, *145*(723), 2385–2403. https://doi.org/10.1002/qj.3568

Zhang, J., Reid, J. S., & Holben, B. N. (2005). An analysis of potential cloud artifacts in MODIS over ocean aerosol optical thickness products. *Geophysical Research Letters*, *32*(15), L15803. https://doi.org/10.1029/2005GL023254